Potential-Induced Plastic Deformations of Nickel Hydrous Electrodes in Alkaline Electrolytes: An *in Situ* Atomic Force Microscopy Study

Yining Hu and Daniel A. Scherson*

Department of Chemistry, Case Western Reserve University, Cleveland, Ohio 44106-7078

Received: January 31, 1997[⊗]

Dimensional changes of α-type nickel hydrous oxide, α-$Ni(OH)_2$(hyd), films electrodeposited on the basal plane of highly oriented pyrolytic graphite, HOPG(bp), electrodes, have been monitored by *in situ* by atomic force microscopy (AFM) in 1 M KOH as a function of the applied potential. Freshly prepared α-$Ni(OH)_2$-(hyd) films were found to consist of conformal sections covered by large numbers of distinctly bright, globular-type features (0.25 μm average diameter), separated by sharply defined crevices. Upon oxidation, the width of the crevices, W_c, increased, whereas the distances between any two globular features, *i* and *j*, within a specific section, r_{ij}, decreased. A statistical analysis involving more than 100 pairs of features from different sections of independent films showed that the relative decrease in r_{ij}, induced by the nominal full oxidation of the film, r_{ij}(ox)/r_{ij}(red), is remarkably constant, 0.06 ± 0.01, and independent of the magnitude of r_{ij}. Plots of W_c obtained from linear AFM scans along an axis normal to the crevice as a function of the extent of oxidation of the films revealed, *within the time scale of the experiments*, a marked hysteresis between the oxidation and subsequent reduction process.

Introduction

Electrochemical processes can, in some instances, give rise to changes in the mechanical properties of electrodes, including modifications in their dimensional characteristics.[1] Although the underlying thermodynamic principles governing many of these effects have been known for quite some time,[1,2] the lack of suitable probes capable of providing direct morphological information *in situ*, i.e. with the electrode under potential control immersed in the electrolyte, has hampered a more detailed characterization of the phenomena involved and, thus, a better identification of the elementary processes responsible for these effects.

This work presents *in situ* atomic force microscopy (AFM),[3,4] as applied to the study of nickel hydrous oxide films electrodeposited on the basal plane of highly oriented pyrolytic graphite, HOPG(bp), and on gold electrodes in 1 M KOH. As shown first by Chen et al.[5] in this laboratory, later by Haring and Kotz,[6] and very recently by Kowal et al.,[7] AFM can be used to monitor *in situ* potential-induced plastic deformations along directions parallel[5] and normal[6,7] to the film surface. The main objective of this study is to exploit the extraordinary capabilities AFM offers to examine in more detail various aspects of the oxidation and reduction of nickel hydrous oxides. Of particular interest is to establish quantitative correlations between morphological changes in the films and their state of charge, or extent of oxidation. The results obtained indicated that the extent of linear contraction, upon a nominal full oxidation of the film, appears consistent with structural information obtained from *in situ* extended X-ray absorption fine structure (EXAFS) for similar films,[8,9] and *ex situ* X-ray diffraction data (XRD)[10,11] for crystalline forms of the material in the oxidized and reduced states. A better understanding of the factors that govern such correlations may be expected to be of practical importance, as it could provide insight into the phenomenon known as *swelling*,[12] which affects adversely the cycle life of rechargeable nickel-based batteries and Ni−H_2 fuel cells.

Experimental Section

α-$Ni(OH)_2$ films supported either on the basal plane of highly oriented pyrolytic graphite, HOPG(bp), or on Au(111) vapor-deposited on optically polished nickel-coated quartz crystal electrodes[13] were prepared by cathodic electrodeposition at constant potential.[14] This procedure was performed in an auxiliary glass cell, using the o-ring of a *fluid cell* for *in situ* AFM measurements (Digital Electronics, Santa Barbara, CA) to define the cross sectional area of the film (ca. 0.3 cm^2). For most of these experiments, the deposition charge (Q_{dep}) was ca. 31 mC/cm^2. Based on the Faradaic efficiency for α-$Ni(OH)_2$(hyd) electrodeposition determined in this[15] and other laboratories,[16] i.e. 2 electrons per single Ni site in the film, this value of Q_{dep} corresponds to 1.7×10^{-7} mol Ni/cm^2.

Freshly grown α-$Ni(OH)_2$(hyd) films were rinsed with pure water and mounted immediately onto the AFM *fluid cell* to avoid excessive dehydration (see below). A piece of platinized platinum wire in the form of a half-loop inserted into the main cell compartment through the cell outlet served as the counter electrode, whereas a conventional Hg/HgO,OH^-(1 M KOH) electrode connected to the cell inlet was used as a reference.

All *in situ* AFM images were collected in 1 M KOH with a Nanoscope II microscope (Digital Instruments) using an E-type scanner and microfabricated cantilevers with a spring force constant of 0.12 N/m. The actual tip consists of a square-base pyramid (4 μm × 4 μm) with an apex angle of 70°, or, equivalently, a height of ca. 2.86 μm. Potential control was achieved with a Pine RDE 4 potentiostat. Electrochemical data were collected in digital form using an A/D board interfaced to an IBM PC computer.

Results and Discussion

Figure 1 shows a typical cyclic voltammogram of an α-$Ni(OH)_2$(hyd)/HOPG(bp) film (Q_{dep} = 31 mC/cm^2) in 1 M KOH, recorded in the *in situ* AFM cell. The overall shape and position of the prominent redox peak, attributed formally to the reaction

[⊗] Abstract published in *Advance ACS Abstracts,* June 1, 1997.

S1089-5647(97)00399-4 CCC: $14.00

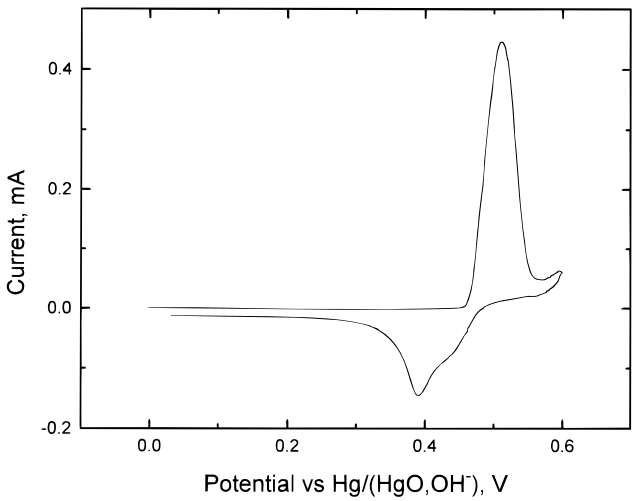

Figure 1. Typical cyclic voltammogram of an α-Ni(OH)$_2$(hyd) film prepared by electrodeposition under potentiostatic conditions (Q_{dep} ca. 31 mC/cm^2) in 1.0 M KOH, recorded in the *in situ* AFM cell.

α-Ni(OH)$_2$ → NiOOH + H$^+$ + e$^-$ as well as those of the peak associated with the subsequent reduction reaction, are in excellent agreement with those reported in this[5] and other laboratories.[6,7] The charge under the reduction peak, Q_{red} (11 mC/cm^2), is somewhat smaller than that expected based on Q_{dep} and calibration curves determined earlier for the deposition of α-Ni(OH)$_2$ films on Au/quartz electrodes (15 mC/cm^2).[13] This discrepancy may be caused, in part, by the difficulties encountered in aligning the o-ring with the electrodeposited area and, also, by the much narrower potential range between the nominal full oxidation of α-Ni(OH)$_2$(hyd) and the onset of dioxygen evolution and/or carbon oxidation for HOPG(bp) compared to Au(111). The latter factor would limit the extent of film oxidation and, therefore, lead to smaller values of Q_{red}.

In situ AFM images (13 μm × 13 μm) of freshly prepared, water-rinsed, α-Ni(OH)$_2$(hyd) films in 1 M KOH at open circuit were found to consist of conformal sections separated by cracks or crevices of widths (W_c), displaying a narrow distribution (range 200−280 nm) peaked at ca. 250 nm (see left panel, Figure 2). This cracking phenomenon appears to occur over periods of time longer than about 30 min, which are often required to set up the *in situ* experiments, and may be ascribed to local contractions of the original film caused by a reequilibration of freshly deposited α-Ni(OH)$_2$(hyd) with the strongly alkaline solution, an effect that could promote dehydration and/or recrystallization. In fact, no crevices could be found for fully hydrated films imaged *ex situ*, i.e. not mounted in the fluid cell, kept under liquid at all times, for which the time involved prior to data acquisition is considerably shorter than that required for *in situ* measurements.

In agreement with our previous report,[5] new crevices developed after the films were polarized at +0.53 V vs Hg/HgO,OH$^-$, i.e. nominally oxidized state, and, as evidenced by the results shown in the center panel, Figure 2, the original crevices found in the fresh films also widened. Following subsequent reduction at 0.0 V, W_c of all crevices decreased markedly, leaving very narrow and, at times, hardly noticeable gaps between adjacent sections of the film (see right panel, Figure 2).

The thickness (τ) of these films (Q_{dep} = 31 mC/cm^2), as determined from the difference in height between the top of the film in an area immediately adjacent to the crevice and the atomically smooth bottom of the crevice, yielded τ = 115 ± 15 nm. This value is in very good agreement with that reported by Haring and Kotz[6] for α-Ni(OH)$_2$ films also grown by electrodeposition from a nitrate solution, containing about the same number of Ni sites/cm^2. (On the basis of the AFM tip dimensions, the maximum measurable depth of a crevice ca. 210 nm wide, about the smallest value obtained experimentally, would be about 150 nm.)

An estimate of the minimum possible thickness (τ_{min}) of a fully oxidized α-Ni(OH)$_2$ layer of Q_{dep} = 31 mC/cm^2 (or equivalently, 1.7 × 10^{-7} mol Ni/cm^2) can be made by assuming that the material is composed of crystalline γ-NiOOH (interlayer distance = 7.2 Å, Ni site density within each layer ca. 2.2 × 10^{-9} Ni sites/cm^2) and, for simplicity, that all layers are parallel to the underlying substrate. On this basis, τ_{min} would be expected to be ca. 55 nm (ca. 77 monolayers), which is about half that measured by *in situ* AFM. At least two factors could account for this discrepancy:

(i) α-Ni(OH)$_2$(hyd) is believed to be composed of very small, highly hydrated, turbostratic crystals lacking long-range order[10] and, therefore, would not be expected to form a compact lattice of the type assumed in the calculation.

(ii) *In situ* Ni K-edge extended X-ray absorption fine structure data (EXAFS) measurements have shown that electrodeposited α-Ni(OH)$_2$ on Au(poly) films polarized at potentials just negative to the onset of oxygen evolution do not undergo complete oxidation.[8]

To the level of resolution of these images, and regardless of the state of oxidation, each of the sections was covered by numerous distinctly bright features, or globular clusters evenly distributed on the film surface. The diameter of the clusters ranged from 0.1 to 0.4 μm, with an average value of ca. 0.25 μm. Similar features, albeit of about half this average diameter, were observed by Haring and Kotz.[6]

Close inspection of these images revealed that the overall spatial disposition of these clusters did not change as a function of the state of oxidation. However, further examination of the actual positions of the clusters *within a given section of the film* did show an increase or a decrease in their relative distance, depending on whether the films were oxidized or reduced, respectively. A more quantitative analysis of this phenomenon was performed by selecting *at random* 11 pairs of images from six independently made films, each pair consisting of images obtained from the same region of a film in both the reduced and oxidized states. Square areas of single sections devoid of visible crevices were then selected from each pair of images using the globular clusters as identification markers. These areas were subsequently enlarged and the relative positions r_{ij} of a number of any two randomly selected clusters, *i* and *j*, both in the reduced (red) and oxidized (ox) films, were carefully measured, using the center point of each cluster as a basis. One such pair of areas is shown in Figure 3 (panel A, reduced; panel B, oxidized).

Sets of r_{ij}(red) and r_{ij}(ox) values were then collected from each of the 11 pairs of images and stored in digital form for further processing. A measure of the relative displacements of clusters induced by a change in the oxidation state was determined by defining a parameter $R_{ij} = r_{ij}(ox)/r_{ij}(red)$. The values of R_{ij} (see open bar histogram in Figure 4) were found to be very similar not only within a given area but also among all the areas examined in independent films, yielding an average of 0.944 ± 0.012. Furthermore, no correlation was found between R_{ij} and $r_{ij}(av) = [r_{ij}(ox) + r_{ij}(red)]/2$. This is clearly evidenced by a plot of R_{ij} vs r_{ij}(av) values obtained from another set of cluster pairs randomly collected from areas of the same set of images, which yielded after a least squares fit, a straight line $R_{ij} = 0.938 - 2.5 \times 10^{-7} r_{ij}$, i.e. virtually zero slope (see Figure 5).

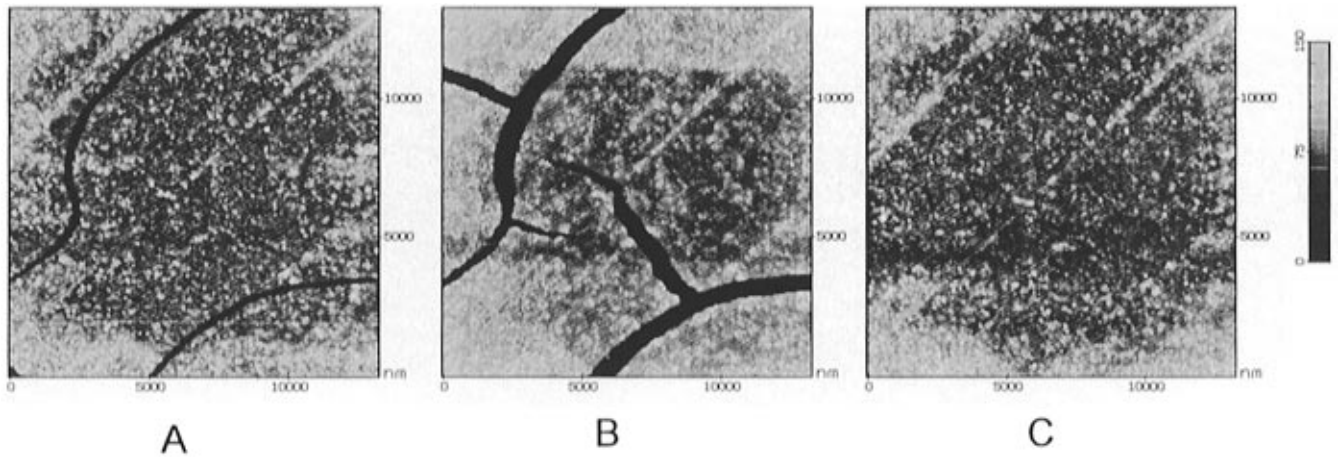

Figure 2. *In situ* AFM images (13 μm × 13 μm) of a freshly prepared, water-rinsed α-Ni(OH)$_2$(hyd) film (Q_{dep} = 31 mC/cm^2) in 1 M KOH at open circuit (panel A), at 0.53 V vs Hg/HgO, OH$^-$, i.e. in the nominally oxidized state (panel B), and at 0.0 V vs HgO, OH$^-$, i.e. fully reduced state (panel C, see Experimental Section for additional details).

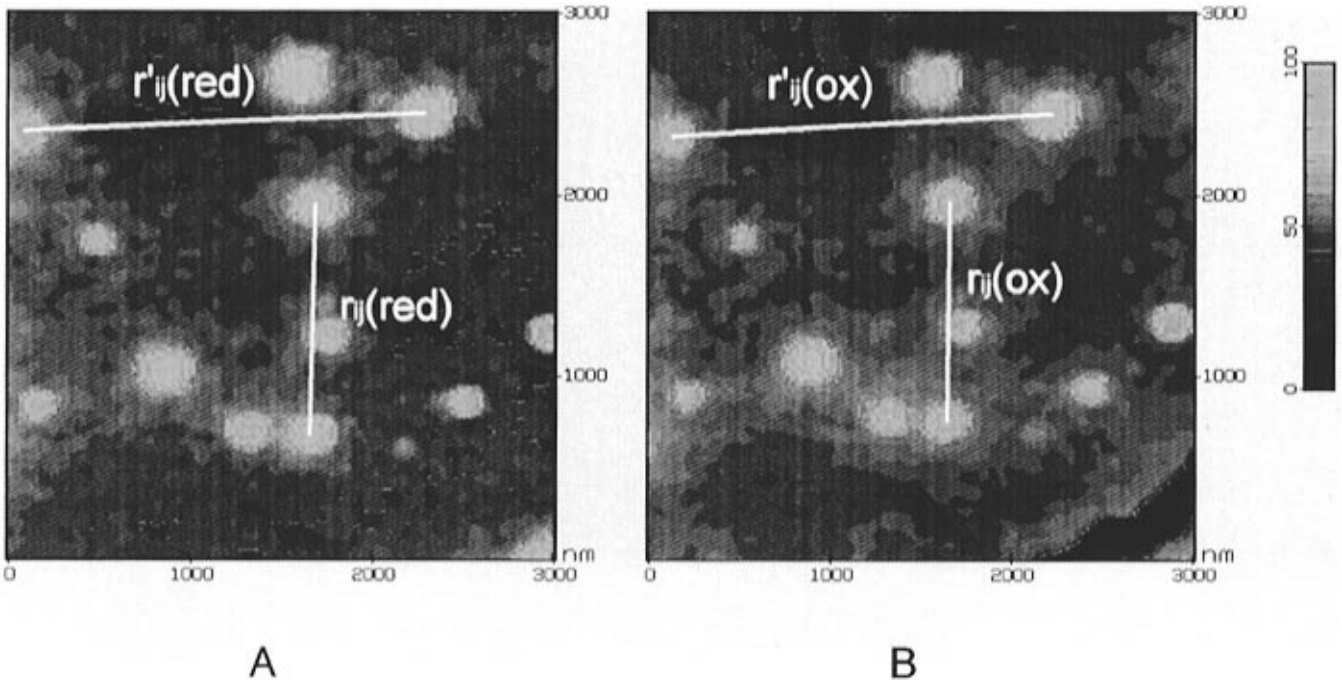

Figure 3. *In situ* AFM images (3μm × 3μm) of areas of a section of a film in the reduced (panel A) and oxidized (panel B) states. r_{ij} and r_{ij}' represent the distances between two arbitrary pairs of clusters in the oxidized (ox) and reduced (red) states.

To establish whether the 11 individual sample sets can be regarded as drawn from the same population, a Student's *t*-test was performed for each set using the formula: $t_i = (x_i - u_0)/(s_i\sqrt{N})$, where x_i and s_i are the mean and standard deviation of set *i*, respectively, u_0 is the population mean, approximated by the simple cumulative average, and N is the total number of data points. The resulting t_i's were checked against the tabulated Student's critical *t* value at the 95% confidence level ($\alpha = 0.05$).

Initially, three sets of data failed the *t*-test, two of which were only marginally outside the range, A_1 and A_2, and the third one A_3, significantly larger than the required *t* value for $\alpha = 0.05$. Further reexamination of the data revealed that the film in two of these sets, A_1 and A_3 (comprising a total of 10 points), as judged by the values of W_c, had not reached full reduction and were, therefore, discarded. New t_i's were calculated using the remaining 96 entries (see histogram with solid bars in Figure 4) to determine the cumulative average (0.942 ± 0.010), yielding in all cases values within the 95% degree of confidence.

The relative spacings between globular clusters, following an oxidation−reduction cycle, were found to be highly reproducible. In fact, the average normalized difference between r_{ij} in the reduced state before (bef) and after oxidation and subsequent reduction (aft), i.e. $\Delta r_{ij} = (r_{ij}(\text{red})_{\text{bef}} - r_{ij}(\text{red})_{\text{aft}})/r_{ij}(\text{red})_{\text{aft}}$, was 0.0013 ± 0.012, with a range of -0.03 to $+0.02$.

These observations strongly suggests that each section of the film is composed of arrays of randomly oriented turbostratic crystals that respond collectively to the change in oxidation state and, therefore, that the interactions between the crystals *within such sections* are relatively strong, forming a cohesive unit, and those between the crystals and the HOPG(bp) are in comparison weaker, allowing entire sections to slide freely along the surface.

Further evidence in support of this view was provided by virtually identical experiments using α-Ni(OH)$_2$ films electrodeposited on Au electrodes, in which case no significant changes in the relative positions of the features were found between the reduced and oxidized states. This contrasting behavior does not imply that α-Ni(OH)$_2$(hyd) on Au(111) does

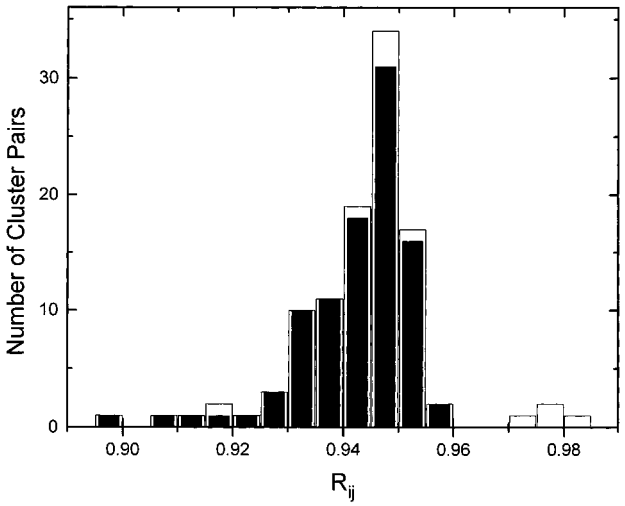

Figure 4. Histogram displaying number of cluster pairs as a function of R_{ij} obtained from all 11 sets (open bars) and after removing the two sets that failed the *t*-test (solid bars).

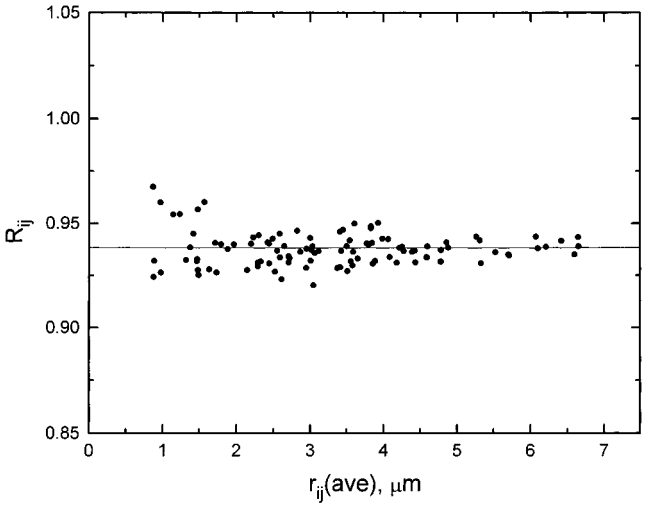

Figure 5. Plot of R_{ij} vs r_{ij} (av) obtained from another set of cluster pairs randomly collected from areas of the same set of images. The straight line, i.e. $R_{ij} = 0.938 - 2.5 \times 10^{-7}\, r_j$, represents the best fit to the data line with virtually zero slope (see Figure 4).

TABLE 1: Structural Parameters for Selected Nickel Hydroxides

	α-Ni(OH)$_2$	γ-NiOOH	% change[a]
interlayer spacing, Å[11]	8.05	7.2	10.5
Ni−Ni distance, Å[8,9]	3.08	2.82	8.4

[a] This parameter represents the extent of contraction upon oxidation along an axis normal (first entry) and parallel (second entry) to the brucite planes.

not contract; rather, the much stronger interactions between the film and Au compared to HOPG(bp) hinder the collective motion of sections of the film large enough for the features to yield, within the level of resolution of these experiments, correlated spatial displacements.

If it is assumed that within the time scale of these experiments the oxidized form of α-Ni(OH)$_2$ yields γ-NiOOH as the product, and that their unit lattice parameters are those obtained from the X-ray diffraction data for the materials in crystalline form, the dimensional changes along and across the individual brucite layers would be expected to be rather similar, i.e. 10.5% and 8.4% (see Table 1). On this basis, and assuming that the individual crystals are randomly oriented with respect to an arbitrary plane, forming a fully isotropic ensemble of turbostratic

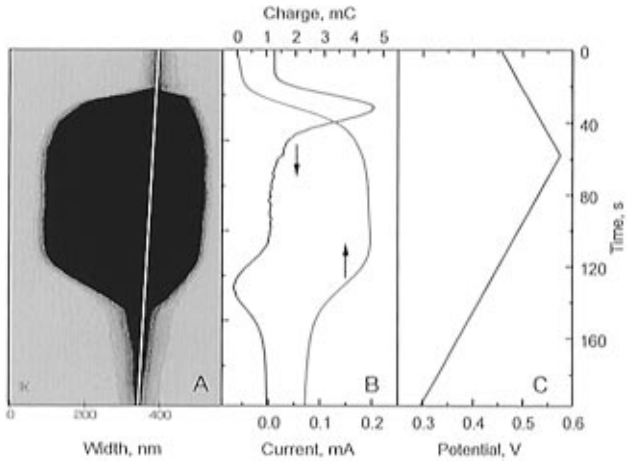

Figure 6. Computer-enhanced *in situ* AFM image (panel A) along an axis normal to the crevice (panel A) obtained during a linear voltammetric scan: current vs time (panel B, thick line), charge vs time (panel B, thin line), potential vs time (panel C).

units, the expected change in linear dimension of each section following oxidation of the film would be 9.1% and, thus, larger than that observed in these AFM experiments, ca. 6%. *In situ* extended X-ray absorption fine structure (EXAFS) performed in this[9] and other[8] research groups indicates that films polarized at the same oxidizing potential as those involved in the AFM measurements display two Ni−Ni shells, $(Ni-Ni)_1$ at a distance of 2.82 Å and $(Ni-Ni)_2$ at 3.08 ± 0.02 Å with relative FT shell amplitudes of 2:1, respectively. These results indicate that for electrodes polarized at potentials just negative to the onset of oxygen evolution the extent to which α-Ni(OH)$_2$(hyd) films can be oxidized does not exceed 60−70%. This being the case, the average dimensional parameters of such partially oxidized films would be in good agreement with the AFM measurements presented in this work.

Much higher values than those predicted by the simple model described above have been reported by Haring and Kotz[6] for virtually identical films as those examined in this work supported on HOPG(bp) (43%) and by Kowal et al.[7] for nickel hydrous oxides formed on nickel electrodes by potential cycling (35%). In both cases, the measurements relied on changes in the height as a function of potential to monitor the extent of plastic deformation. One possible explanation for such large differences may be found in optical artifacts derived from changes in the index of refraction of the media induced by changes in the electrolyte concentration in the neighborhood of the counter electrode, which at least in our experimental arrangement is located close to the path of the reflected laser beam. As shown in Appendix A, a relative increase in the index of refraction associated with an increase in the local concentration of KOH would lead to height changes during an oxidation/reduction cycle as measured by the AFM microscope, which are larger than those derived from purely mechanical deformations.

A series of experiments were performed in which the width of the crevice, W_c, was imaged by *in situ* AFM as the potential was scanned over a range that included the redox transition. For these measurements, images were collected at a higher resolution (1 μm × 1 μm) along an axis normal to the crevice (*x*-scan) over a length somewhat larger than the maximum width of the crack, during a voltage scan, while keeping the *y*-axis scan disabled.

One such set of results is shown in Figure 6, where the *in situ* AFM image (panel A) has been computer-enhanced for clarity. Also plotted in this figure is the current as a function of time during the linear cyclic scan (thick line, panel B) and

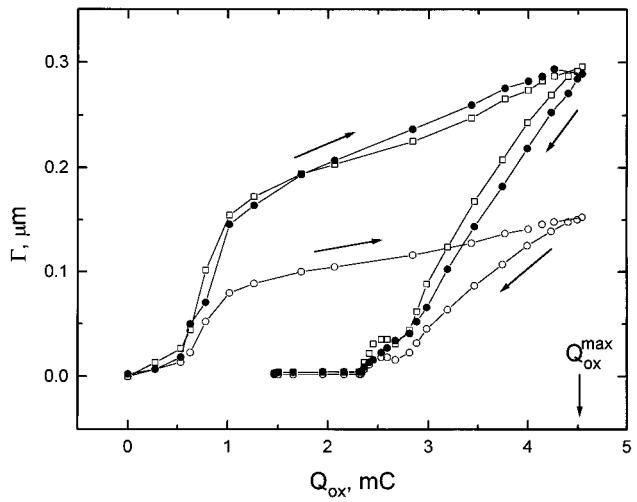

Figure 7. Plots of Γ vs Q_{ox} obtained during oxidation (right pointing arrow) and reduction cycle (left pointing arrow) for the left (solid circles) and right (open circles) sections of the film in panel A, Figure 6. The open squares curve was obtained after normalizing the curve in open circles using Γ at Q_{ox}^{max} as a basis.

the oxidation charge Q_{ox} determined by a straightforward integration (thin line, panel B). The potential vs time curve is shown in panel C in this figure. It becomes evident from these data that the changes in dimensionality are directly related to corresponding changes in the state of oxidation and reduction of the film; that is, W_c remains unaltered until the onset of the oxidation.

A more quantitative analysis of these results could be pursued by plotting W_c, as a function of the extent of oxidation of the film Q_{ox}, shown by the thin line in panel B, Figure 6. However, W_c represents the sum of contributions due to two adjacent sections of the film, each undergoing independently contraction (or expansion) as the oxidation (or reduction) proceeds. Hence, it appears more appropriate to analyze the extent of contraction Γ for each individual section using the position of the crevice in the reduced state as a common reference point (see white line in panel A, Figure 6). Figure 7 shows plots of Γ vs Q_{ox} obtained during a full oxidation and reduction cycle for the left (solid circles) and right (open circles) sections of the film. The overall shape of the curves obtained for each section was found to be essentially identical, as evidenced by the near coincidence of the two sets of data obtained upon normalizing the lower set of data by an arbitrary factor (see open squares).

These results clearly show that *within the time scale of these experiments*, the dimensional characteristics of the films are not uniquely determined by their state of charge. In particular, the Γ vs Q_{ox} curves during oxidation were characterized by regions of slow, fast, and intermediate rates of contraction in the ranges $0 < Q_{ox} < 10\%Q_{oxmax}$, $10 < Q_{ox} < 20\%Q_{ox}^{max}$, and $Q_{ox} > 20\%Q_{ox}^{max}$, respectively, where Q_{ox}^{max} represents the maximum charge of oxidation, i.e. ca. 4.5 mC for this film. The initial rate of expansion observed upon reduction of nominally fully oxidized films, however, was found to be about twice that observed within the same range of Q_{ox} values, indicating that the reduction of about half of the film occurs without measurable lateral changes in morphology. It is interesting to note that the rate of expansion is virtually constant during the initial stage of reduction down to $Q_{ox} = 60\%Q_{ox}^{max}$. Beyond that point, and especially for the right section of the film, the resolution of the images is poor; hence the corresponding values of Γ are subject to relatively large uncertainties.

A thermodynamic analysis of plastic deformations of the type found for α-$Ni(OH)_2$(hyd) films cannot be performed based on the mechanical/electrochemical formalism described by Bowden et al.[2] These difficulties stem from the fact that the state of the system is not prescribed uniquely by the potential, as the extent of contraction (or expansion) depends on the previous history, as illustrated by the hysteresis cycle in Figure 7. A rigorous treatment of systems displaying this type of behavior must rely instead on theoretical arguments, such as those invoked by Everett and co-workers[17] in their work on metal hydrides, where the hysteresis involves changes in the volume of the material, associated with the non-electrochemical insertion of hydrogen into the metal, induced by changes in the partial pressure of hydrogen in the surrounding environment.

Other Observations. The stability of nickel hydrous films in the nominally oxidized state was examined by first recording an image with the electrode polarized at 0.53 V vs Hg/HgO, OH^- (see Figure 8), just prior to disconnecting the potentiostat, and a second image 90 min thereafter. As can be clearly discerned, W_c decreased markedly, indicating that the film had undergone spontaneous reduction, otherwise known as *self-discharge*. The same conclusion was made based on *in situ* X-ray absorption fine structure (XAFS) measurements of virtually identical films supported on Au (or gold oxide), in which the absorption edge shifted toward lower binding energies when the cell was disconnected.[18]

Additional experiments in which α-$Ni(OH)_2$(hyd) films were imaged after being cycled between 0.0 and 0.57 V vs Hg/HgO,$^-$ at a rate of 5 mV/s for 18 h, and subsequently polarized at 0.6 V showed the films to undergo very slow contraction. One possible explanation for this effect may be found in the slow transformation of α- to *β*-$Ni(OH)_2$(hyd), which, as shown by QCM measurements in this laboratory, appears to involve a radically different mechanism of ionic transport through the lattice compared to the α-form. In contrast to the behavior found for α-$Ni(OH)_2$(hyd), nickel hydrous oxide films on HOPG(bp) prepared from mixtures of $Ni(NO_3)_2$ and $Co(NO_3)_2$ solutions in the ratio of 9:1,[9] examined in 1 M KOH, showed markedly fewer crevices (following preparation and rinsing) and values for W_c obtained *in situ*, which were independent of the state of charge. This phenomenon suggests that cobalt sites in the nickel hydrous oxide lattice[9] decrease the apparent volume change induced by corresponding changes in oxidation state and could, thus, explain, at least in part, the beneficial effects associated with the presence of this metal additive to the rechargeability of technical nickel oxide electrodes.

Summary

In situ AFM images obtained in 1 M KOH have shown that changes in the oxidation state of α-$Ni(OH)_2$(hyd) films prepared by electrodeposition are accompanied by changes in the morphology of the material. In particular, the films undergo contraction, i.e. ca. 6%, during oxidation and expansion following subsequent reduction.

A statistical analysis of the spatial distribution of globular clusters as a function of the state of charge indicates that large sections of the film respond as a single unit to changes in oxidation state. This observation suggests that *within a section* the interactions between globular species are relatively strong and those between the film and the HOPG(bp) substrate are weak, allowing the sections to slide along the surface during changes in oxidation state.

Plots of the extent of contraction as a function of the state of charge recorded over a voltammetric cycle in the range 0.03−0.57 V vs Hg/HgO, OH^- showed a pronounced hysteresis, indicating that at least *within the time scale of the experiments* the coefficients of plastic deformation are different depending on whether the films are first reduced or oxidized.

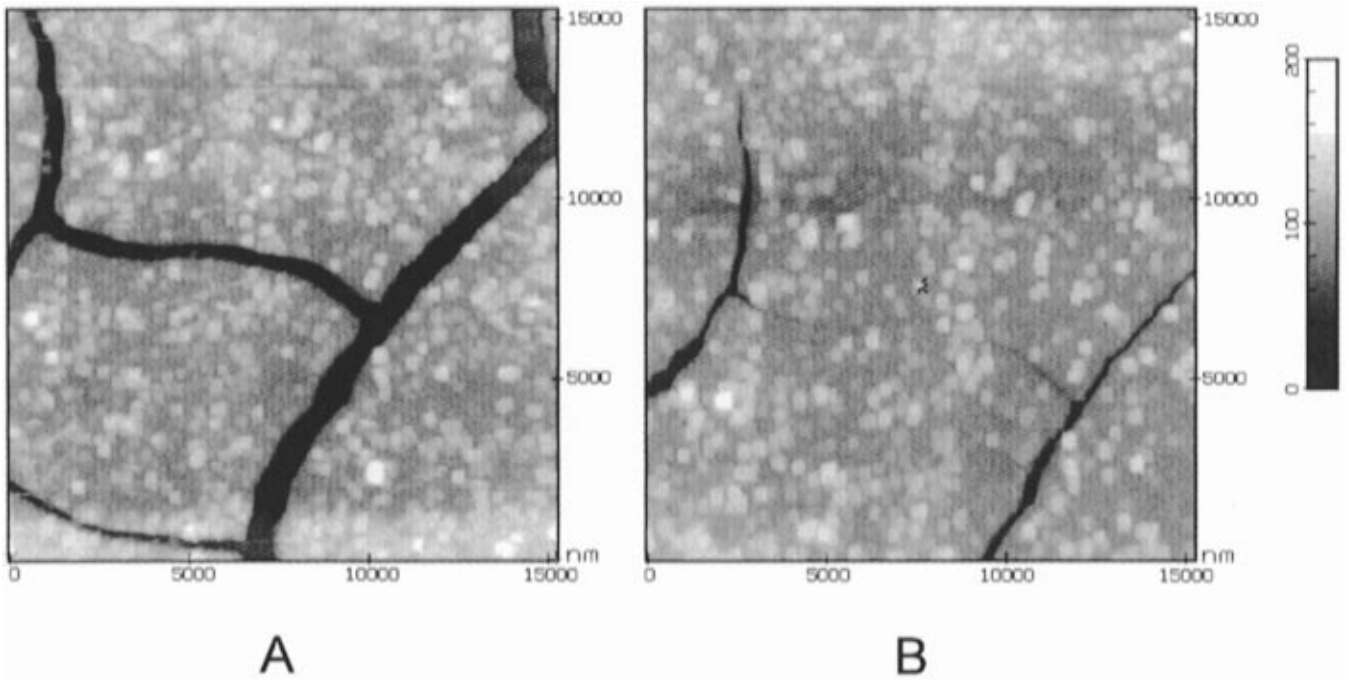

Figure 8. *In situ* AFM images (15 μm × 15 μm) of nominally fully oxidized α-Ni(OH)$_2$(hyd) film polarized as 0.53 V vs Hg/HgO, OH$^-$ and of the same film obtained 90 min without potential control (see text for details).

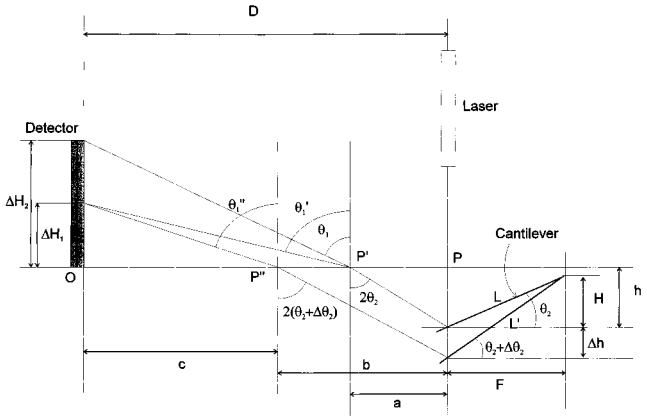

Figure 9. Schematic diagram of an experimental setup for *in situ* atomic force microscopy measurements.

Acknowledgment. This work was supported by the Department of Energy, Office of Basic Energy Sciences.

Appendix A

Consider the *in situ* AFM experimental arrangement shown in Figure 9, in which the laser beam crosses the air/electrolyte interface at normal incidence at a point *P* and reflects off the top surface of an immersed cantilever (directly above its tip) at a distance *h* normal to the surface of the liquid. Assume, furthermore, that the cantilever makes an angle θ_2 with respect to the interfacial plane. Due to refraction, the reflected beam will emerge from the solution at an angle θ_1 with respect to the normal to liquid surface. On the basis of classical optics, the angle of the emerging beam θ_1 can be calculated from Snell's law, i.e.

$$n_1 \sin \theta_1 = n_2 \sin 2\theta_2 \tag{1}$$

where n_1 and n_2 are the reflective indices of air and the electrolyte, respectively. A displacement in the cantilever position induced by a small change in the height of the specimen being imaged denoted as Δh and shown without loss of generality, as a height decrease in Figure 9, would elicit a corresponding change in θ_2, defined as $\Delta\theta_2$ in that figure, and, consequently, in the angle at which the reflected beam will emerge from the solution. Hence, the emerging angle in this new configuration θ_1' may be written as

$$\theta_1' = \arcsin\{(n_2/n_1)\,(\sin 2(\theta_2 + \Delta\theta_2)\} \tag{2}$$

Since $\Delta\theta_2 = \arctan[(H + \Delta h)/F] - \arctan(H/F)$, where $F = L \cos \theta_2$ and L is the length of the cantilever, the change in the position of the beam at the detector placed (for simplicity) at a distance D parallel to the original incident laser beam and denoted as ΔH ($=\Delta H_2 - \Delta H_1$) may be shown to be given by

$$\Delta H = (D - h \tan 2\theta_2)/\tan \theta_1 - c/\tan \theta_1' \tag{3}$$

However, the same detector response would be obtained by increasing the index of refraction of the solution above the cantilever at fixed height, i.e. $\Delta h = 0$. In fact, the relative change in n_2, $\Delta n_2/n_2$, capable of eliciting such a response can be calculated from Snell's law:

$$n_1 \sin \theta_1'' = (n_2 + \Delta n_2) \sin \theta_2 \tag{4}$$

which after simple algebraic manipulations may be shown to yield

$$\Delta n_2/n_2 = (n_1/n_2)(\sin \theta_1''/\sin 2\theta_2) - 1 \tag{5}$$

where

$$\theta_1'' = \arctan\{[(D - a)/c] \tan \theta_1'\} \tag{6}$$

$$\theta_1' = \arcsin\{(n_2/n_1)[2(\Delta h/F) \cos 2\theta_2 + \sin 2\theta_2]\} \tag{7}$$

$$a = h \tan 2\theta_2 \tag{8}$$

$$c = D - (h + \Delta h) \tan 2(\theta_2 + \Delta\theta_2) \tag{9}$$

and Δh is the change in height observed for $\Delta n_2 = 0$.

For example, assuming reasonable values for all parameters involved, i.e. $n_1 = 1$, $n_2 = 1.33$, $h = 1$ mm, $D = 2$ cm, $l = 170$ μm, and $\theta_2 = 10°$, $\Delta h = 5$ nm and 25 nm correspond to $\Delta n_2/n_2 = 1.593 \times 10^{-4}$ and $\Delta n_2/n_2 = 7.965 \times 10^{-4}$, respectively. Although it is not possible to assess quantitatively the expected change in n_2 around the counter electrode following oxidation of the film, the expected increase in the concentration of KOH would be consistent with a corresponding increase in n_2, as the model predicts, leading to larger measured values of the height change observed experimentally.

References and Notes

(1) Parsons, R. In *Comprehensive Treatise of Electrochemistry*; Bockris, J. O'M., Conway, B. E., Yeager, E. B., Eds.; Plenum Press: New York, 1980; Vol. 1, p 1.

(2) (a) Bowen, E. F.; Dautarts, M. F.; Evans, J. F. *J. Electroanal. Chem.* **1987**, *219*, 49. (b) Dautarts, M. F.; Bowen, E. F.; Evans, J. F. *J. Electroanal. Chem.* **1987**, *219*, 70.

(3) Quate, F. *Surf. Sci.* **1994**, *299/300*, 980.

(4) (a) Manne, S.; Hansma, P. K.; Massie, J.; Elings, V. B.; Gewirth, A. *Science* **1991**, *251*, 131. (b) Chen, C. H.; Gewirth, A. *J. Am. Chem. Soc.* **1991**, *113*, 6049.

(5) Chen, R.; Mo, Y.; Scherson, D. A. *Langmuir* **1994**, *10*, 3931.

(6) Haring, P.; Kotz, R. *J. Electroanal. Chem.* **1995**, *385*, 273.

(7) Kowal, A.; Niewiara, R.; Peronczyk, B.; Haber, J. *Langmuir* **1996**, *12*, 2332.

(8) (a) Pandya, K. I.; Hoffman, R. W.; McBreen, J.; O'Grady, W. E. *J. Electrochem. Soc.* **1990**, *137*, 383. (b) O'Grady, W. E.; Pandya, K. I.; Swider, K. E.; Corrigan, D. A. *J. Electrochem. Soc.* **1996**, *143*, 1613.

(9) Kim, S.; Tryk, D. A.; Antonio, M. R.; Carr, R.; Scherson, D. A. *J. Phys. Chem.* **1994**, *98*, 10269.

(10) Oliva, P.; Leonardi, J.; Laurent, J. F.; Delmas, C.; Braconnier, J. J.; Figlarz, M.; Fievet, F.; Guibert, A. *J. Power Sources* **1982**, *8*, 229.

(11) McBreen, J. In *Modern Aspects of Electrochemistry*; White, R. E., Bockris, J. O'M., Conway, B. E., Eds.; Plenum Press: New York, 1990; Vol. 21, p 29.

(12) Oshitani, M.; Takayama, T.; Takashima, K. *J. Appl. Electrochem.* **1986**, *16*, 403.

(13) Mo, Y.; Hwang, E.; Scherson, D. A. *Anal. Chem.* **1995**, *67*, 2415.

(14) Corrigan, D. A. *J. Electrochem. Soc.* **1987**, *134*, 377.

(15) Mo, Y.; Hwang, E.; Scherson, D. A. *J. Electrochem. Soc.* **1996**, *143*, 37.

(16) Desilvestro, J.; Corrigan, D. A.; Weaver, M. J. *J. Electrochem. Soc.* **1988**, *135*, 885.

(17) Flanagan, T. B.; Park, C. N.; Everett, D. H. *J. Chem. Educ.* **1987**, *64*, 944.

(18) Hu, Y.; Mo, Y.; Bae, I. T.; Scherson, D. A. Extended Abstracts Electrochemical Society Meeting, Spring 1996, Abstract 74; *Ibid.* Fall 1996, Abstract 312, Hu, Y.; Mo, Y.; Bae, I. T.; Antonio, A.; Scherson, D. A. (in preparation).